Dose-response modeling reveals multifaceted molecular responses to low-dose radiation in human white blood cells

Khilji, Saadia; Vuong, Ngoc Q.; Williams, Andrew; Fulton, Kelly M.; Baay, Isabel; Twine, Susan M.; Meier, Matthew J.; Kumarathasan, Premkumari; Wilkins, Ruth C.; Yauk, Carole L.; Chauhan, Vinita

Publisher's version / Version de l'éditeur:
https://doi.org/10.1080/09553002.2025.2540354
International Journal of Radiation Biology, pp. 1-14, 2025-08-20

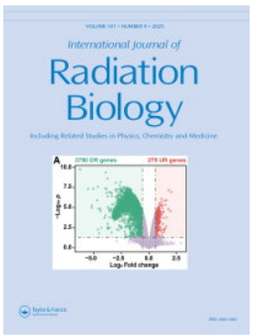

International Journal of Radiation Biology

ISSN: 0955-3002 (Print) 1362-3095 (Online) Journal homepage: www.tandfonline.com/journals/irab20

Dose-response modeling reveals multifaceted molecular responses to low-dose radiation in human white blood cells

Saadia Khilji, Ngoc Q. Vuong, Andrew Williams, Kelly M. Fulton, Isabel Baay, Susan M. Twine, Matthew J. Meier, Premkumari Kumarathasan, Ruth C. Wilkins, Carole L. Yauk & Vinita Chauhan

To cite this article: Saadia Khilji, Ngoc Q. Vuong, Andrew Williams, Kelly M. Fulton, Isabel Baay, Susan M. Twine, Matthew J. Meier, Premkumari Kumarathasan, Ruth C. Wilkins, Carole L. Yauk & Vinita Chauhan (20 Aug 2025): Dose-response modeling reveals multifaceted molecular responses to low-dose radiation in human white blood cells, International Journal of Radiation Biology, DOI: 10.1080/09553002.2025.2540354

To link to this article: https://doi.org/10.1080/09553002.2025.2540354

INTERNATIONAL JOURNAL OF RADIATION BIOLOGY
https://doi.org/10.1080/09553002.2025.2540354

Taylor & Francis
Taylor & Francis Group

ORIGINAL ARTICLE

OPEN ACCESS Check for updates

Dose-response modeling reveals multifaceted molecular responses to low-dose radiation in human white blood cells

Saadia Khilji[a], Ngoc Q. Vuong[b], Andrew Williams[c], Kelly M. Fulton[d], Isabel Baay[d], Susan M. Twine[d,e], Matthew J. Meier[c], Premkumari Kumarathasan[c], Ruth C. Wilkins[a], Carole L. Yauk[f] and Vinita Chauhan[a]

[a]Consumer and Clinical Radiation Protection Bureau, Health Canada, Ottawa, Ontario, Canada; [b]Radiation Protection Bureau, Health Canada, Ottawa, Ontario, Canada; [c]Environmental Health Science and Research Bureau, Health Canada, Ottawa, Ontario, Canada; [d]Human Health Therapeutics Research Center, National Research Council Canada, Ottawa, Ontario, Canada; [e]Department of Biology, Carleton University, Ottawa, Ontario, Canada; [f]Department of Biology, University of Ottawa, Ottawa, Ontario, Canada

ABSTRACT

Background: The current radiation protection framework extrapolates health risks from high-dose exposures based on a linear, no-threshold model. However, empirical data on molecular effects below 0.1 Gy are lacking, creating uncertainties in risk assessments. To address this, we used benchmark dose (BMD) modeling, commonly applied in chemical hazard assessment, to analyze gene and protein expression changes in human white blood cells, providing insights into dose-response relationships following low-dose radiation (LDR) exposure.

Methods: Blood samples were collected from 14 participants (6 females, 8 males). Lymphocytes were isolated, cultured, and exposed to X-irradiation at nine doses (0–6 Gy) at 0.05 Gy/min. Transcriptomic and proteomic changes were assessed 24 h post-exposure. BMD modeling was applied to each endpoint, and the data were grouped into distinct dose-response patterns. Pathway analysis identified cellular functions associated with these patterns, offering insight into the biological effects of LDR.

Results: BMD modeling identified 1,204 genes and 168 proteins with dose-response relationships, with median BMD lower confidence limits (BMDLs) of 1.38 Gy and 0.21 Gy, respectively. Transcriptional and proteomic responses exhibited complex patterns, including exponential, biphasic, and hypersensitivity responses, with peak activity between 0.05–0.25 Gy, followed by a decline or plateau. Pathway analysis revealed changes in genes and proteins related to DNA damage, cell cycle, cellular stress, metabolism, immune function, and cancer, with DNA damage response genes showing BMDLs below 0.1 Gy.

Conclusions: This study shows that molecular dose-response relationships can be complex and non-linear, emphasizing the need for further research to better understand the effects of LDR.

ARTICLE HISTORY
Received 26 March 2025
Revised 27 June 2025
Accepted 22 July 2025

KEYWORDS
Low-dose radiation; benchmark dose modeling; transcriptomics; proteomics

Introduction

Over the past several decades, the number of people exposed to chronic low-dose radiation (LDR) (<0.1 Gy) has steadily increased, primarily due to the extensive use of medical imaging procedures, with additional contributions from occupational and environmental sources (Tharmalingam et al. 2017; Karami and Gholami 2018; UNSCEAR 2021). Given, the widespread nature of these exposures, even small associated risks could have significant public health implications, making it important to understand the risks of LDR.

Epidemiological studies have been central to understanding the health effects of ionizing radiation, contributing to the widespread adoption of the linear no-threshold (LNT) model as the foundation of current radiation protection guidelines (Laurier et al. 2023). The LNT model, largely based on high acute dose exposures such as those observed in the Life Span Study of atomic bomb survivors, suggests that any radiation dose, regardless of magnitude, linearly increases the risk of cancer and genetic mutations (Preston et al. 2007; UNSCEAR 2012; Laurier et al. 2023). While the LNT model offers a pragmatic framework for risk assessment, it faces limitations when applied to low-dose exposures (Cardarelli and Ulsh 2018; Ji et al. 2019; Pennington and Siegel 2019). Additionally, epidemiological studies often lack the statistical power to reliably detect increased risks at lower doses due to the small effect sizes and the confounding factors present in population-level data (Little and Muirhead 1996; Wakeford 2009; Boice 2017). To address these gaps, mechanistic studies, particularly multi-omic analyses of gene and protein responses, are necessary for reducing uncertainties regarding the health impacts of LDR. By

CONTACT Vinita Chauhan vinita.chauhan@hc-sc.gc.ca Consumer and Clinical Radiation Protection Bureau, Health Canada, 775 Brookfield Road, PL 6303B, Ottawa, Ontario K1A 1C1, Canada

Supplemental data for this article can be accessed online at https://doi.org/10.1080/09553002.2025.2540354.

bridging molecular-level responses with epidemiological findings, omics-based studies can provide comprehensive insights into gene, protein, and metabolic variations that link to health outcomes (Everson and Marsit 2018; Roberts et al. 2024).

BMD modeling is a statistical approach initially developed for toxicological studies to identify the dose of a substance that triggers a specific biological response, known as the benchmark response (BMR) (e.g. a 10% change in an endpoint of interest) (Crump 1984). Unlike conventional methods such as No-Observed Adverse Effect Level (NOAEL) or Lowest-Observed Adverse Effect Level (LOAEL), which rely on fixed dose points, BMD modeling examines the entire dose-response curve to determine the dose associated to the BMR (Haber et al. 2018). This method enables the identification of the lowest dose of activity for apical or molecular responses and provides a more accurate determination of points of departure (PODs) (Wignall et al. 2014; Hardy et al. 2017; Reardon et al. 2023). As a result, it has become the preferred approach for establishing health-based dose guidance values in chemical exposure assessments. Alongside the BMD, the lower confidence limit (BMDL) and upper confidence limit (BMDU) are also calculated, representing a user-defined confidence interval around the BMD, with the BMDL frequently used to establish reference doses in chemical risk assessments (Food and Agriculture Organization of the United Nations and the World Health Organization 2009).

Although widely used in toxicology, the application of BMD modeling to radiation research is relatively recent. This approach has been used to identify gene and pathway sensitivities associated with radiation-induced outcomes, such as cataract formation and UV-induced skin cancer, providing dose estimates that align with human exposure limits derived from animal models (Qutob et al. 2018; Chauhan et al. 2019). Importantly, as advances in software have facilitated the application of BMD modeling to high-dimensional -omic datasets, researchers have been able to calculate BMD values for individual genes, proteins, and their associated pathways (Phillips et al. 2019; Liu et al. 2023; Vuong et al. 2025). BMD modeling has also been applied to transcriptomic and proteomic responses in human white blood cells exposed to radiation, enabling the identification of sensitive pathways and quantitative PODs relevant to an adverse outcome pathway (AOP) described radiation-induced acute myeloid leukemia (Vuong et al. 2025). Collectively, these studies emphasize the value of BMD modeling in advancing our understanding of molecular responses and potential health outcomes of radiation exposure.

Despite its potential, previous studies leveraging publicly available radiation omics datasets have often fallen short due to a limited dose range or a focus on high-dose exposures, which are less relevant for low-dose risk assessment (Chauhan et al. 2021; Stainforth et al. 2022; Vuong et al. 2025). To address these gaps, we aimed to generate robust dose-response data by isolating white blood cells (WBCs) from the blood of 14 healthy human donors and exposing them to X-ray radiation across a dose range of 0.05 to 6 Gy at a dose rate of 0.05 Gy/min. Transcriptomic and proteomic changes were assessed using Tempo-Seq and mass spectrometry analysis, at 24 h post-exposure. We then applied BMD modeling to calculate gene- and pathway-specific BMD values and integrated these with distinct dose-response clusters to identify the lowest dose of activity for key molecular responses.

Methods

The methods in this study closely follow those described by Vuong et al. (2025).

Materials

The materials and equipment used in this study are organized by supplier, along with their corresponding catalog numbers. Eppendorf: 50 mL conical tubes (0030122178), 15 mL conical tubes (0030122151). HyClone: deionized phosphate-buffered saline (1X DPBS, SH30028LS). Gibco: RPMI 1640 (21870-076), white-wall 96-well plates (655073). Millipore Sigma: fetal bovine serum (FBS, F1051), L-glutamate/Penicillin-Streptomycin (G1146), Trypan Blue (T8154-20mL), Histopaque®-1077 (10771), 50 mL Accuspin tubes (A2055-10EA). Thermo Fisher Scientific: protease inhibitor (78429), 60 mm culture dishes (130181). Bio-Rad: RC DC™ Protein Assay Kit II (5000122). Fisher Scientific: 0.5 mL microcentrifuge tubes (14-666-332). BioSpyder: TempO-Seq S1500+ kit. Beckman: DxH 520 Hematology Analyzer. Promega: Trypsin Gold (Mass Spectrometry Grade, V5280), ATP assay kit (PR-G7571).

White blood cell (WBC) isolation

Peripheral blood samples were collected from healthy adult volunteers with informed consent from each participant and approval from Health Canada's Research Ethics Board (protocol REB 2002–0012H). Donors were self-reported non-smokers in good health, with no known illnesses or exposure to medical ionizing radiation within the previous 12 months (8 males, 6 females, aged 22–49 years). Blood samples were collected into EDTA vacutainer tubes and processed for WBC isolation using Histopaque®-1077 (Millipore Sigma) (Böyum 1968) following the manufacturer's protocol, as described previously (Vuong et al. 2025). The resulting WBC pellet was resuspended in culture medium, and the cell concentration was adjusted to 1.0×10^6 cells/mL. The isolated WBCs were then divided into aliquots of 2.0×10^6 cells/culture dish/dose.

Irradiations

WBCs were exposed to X-ray irradiation using a cabinet X-ray machine (X-RAD 320, Precision X-Ray Inc., North Branford, CT), operating at 250 kVp and 12.5 mA with filter F2 (0.75 mm Sn + 0.25 mm Cu + 1.5 mm Al; half-value layer [HVL] approximately 3.7 mm Cu). Cells were irradiated at nine different doses (0.0, 0.05, 0.1, 0.25, 0.5, 1.0, 2.0, 4.0, and 6.0 Gy) with a dose rate of 0.05 Gy/min, as previously

described (Vuong et al. 2025). A PTW TW30010-10 ion chamber and a T10002 electrometer (PTW, Freiburg, Germany) were used to determine the dose rate. Twenty-four hours following exposure, cell suspensions were reserved for subsequent analyses: Trypan Blue Exclusion (TBE) assay (2.0×10^4 cells), cell counts (2.0×10^4 cells), ATP concentration measurements (7.5×10^4 cells), transcriptomic analysis (5.0×10^5 cells), and proteomic analysis (1.4×10^6 cells).

ATP assay

ATP concentration was measured following the manufacturer's protocol. In brief, 75 μL of ATP reagent was added to each sample in a white-wall 96-well plate, which was then covered with foil and incubated on an orbital shaker for 15 min at room temperature. Luminescence was subsequently measured (Agilent BioTek Cytation 5 Cell Imaging Multimode Reader).

Trypan blue exclusion (TBE) assay

A 10 μL aliquot of cell suspension was mixed with 10 μL of 0.4% Trypan Blue solution (1:1 ratio). Then, 10 μL of the stained mixture was loaded onto a hemocytometer. Viable (unstained) and non-viable (blue-stained) cells were counted manually under a light microscope. Cell viability was calculated as: % viability = (number of viable cells/total number of cells) × 100.

Transcriptomic analysis

Twenty-four hours post-irradiation, 100,000 cells (in DPBS) were combined with TempO-Seq™ Enhanced Lysis Buffer (BioSpyder Technologies). The samples were incubated at 37 °C for 10 min and subsequently stored at −80 °C until further analysis.

TempO-Seq™ oligo mix was used to hybridize mRNA, followed by nuclease digestion, ligation, and barcoding for multiplexing. The resulting amplicons were purified using a PCR clean-up kit (Clontech) and sequenced on an Illumina NextSeq® 500. Sequencing data were demultiplexed and processed using an in-house pipeline developed for regulatory toxicology studies using transcriptomic data, as described previously (Verheijen et al. 2022). The data that support the findings of this study are openly available in the Gene Expression Omnibus (GEO) database at https://www.ncbi.nlm.nih.gov/geo/query/acc.cgi?acc=GSE260589 (accession number GSE260589), and the code used for analysis is accessible at https://github.com/R-ODAF/R-ODAF_Health_Canada.

The resulting gene counts were normalized as counts per million (CPM) to account for differences in sequencing depth across samples. Gene expression analysis was conducted using a generalized linear mixed model (GLMM) with a negative binomial distribution, which is appropriate for modeling overdispersed count data typical of RNA-seq experiments. The model was implemented using the glmer.nb() function from the lme4 R package (Bates et al. 2015) with subject included as a random effect to account for inter-individual variability. Fixed effects included dose, dose rate, and their interaction. Comparisons to control samples were performed using the doBy R package (Højsgaard and Halekoh 2023), which facilitated estimation of pairwise contrasts. Estimated differences were exponentiated to obtain fold changes, then linearized, and standard errors were approximated using the delta method.

Proteomic analysis

Twenty-four hours post-irradiation, 700,000 cells were washed with DPBS containing protease inhibitor and stored as a pellet at −80 °C. For protein extraction, cell pellets were lysed in a DTT-supplemented buffer, sonicated, and the supernatant was collected for protein quantification. Alkylation was done with 200 mM iodoacetamide, followed by acetone precipitation at −20 °C. The protein pellet was resuspended in ammonium bicarbonate, digested overnight with trypsin at 37 °C, and the digestion was quenched with 0.1% formic acid, yielding a final peptide concentration of 0.1 μg/μL. Samples were stored at −80 °C until analysis by nano-liquid chromatography tandem mass spectrometry (nLC-MS/MS).

Following digestion, 10 µL of the peptide digest was analyzed by nLC-MS/MS using an UltiMate 3000 HPLC system (Dionex) coupled to an Orbitrap Exploris 480 mass (Thermo Fisher) equipped with a FAIMS Pro Duo Interface (using alternating −50/−70 CV). Peptides were desalted on a C18 trap column (300 µm × 4 mm Pepmap Neo; Dionex) and then separated using a BEH C18 column (100 µm × 10 cm, 1.7 µm, 100 Å; Waters). For the gradient elution, solvent A (A) contained 0.1% formic acid in HPLC-grade water while solvent B (B) contained 0.1% formic acid in acetonitrile. The gradient used went from 1 to 40% B over 61 min and then from 40 to 85% B over 3 min, before returning to 1% B over 1 min to re-equilibrate for an additional 8 min. The MS spectra were acquired in the Orbitrap (resolution of 15,000) while the higher energy collision dissociation (HCD) fragmentation spectra were acquired in the ion trap using data dependent analysis (DDA).

For protein identification and quantification, the mass spectrometry files were analyzed using FragPipe (version 20.0). Within FragPipe, MS Fragger (version 3.8) (Kong et al. 2017) was used to determine protein identification by searching against the NCBI Homo sapiens protein sequence database (with decoys added) and validation was achieved with PeptideProphet selected in Philosopher (version 4.4.0) (da Veiga Leprevost et al. 2020). Relative quantification of identified proteins was executed with IonQuant (version 1.9.0) (Yu et al. 2020) using the match between runs (MBR) feature enabled. The false discover rate was set to 0.05 with retention time tolerances of 2 min.

For differential protein analysis, total protein intensities were quantified using IonQuant with match-between-runs (MBR) and normalized to β-actin. Missing values were imputed using the k-nearest neighbors (kNN) algorithm with k = 5. The detection limit was estimated based on the smallest nonzero value of protein intensity, with values

below this threshold set to zero. Data were then further normalized to the average of two control samples. After merging subject data, additional missing values were imputed using kNN. A linear mixed model (LMM) was applied to analyze differences between dose groups while subject was treated as a random effect. Comparisons to controls were conducted using the doBy R package, and fold changes were calculated, with standard errors estimated via the delta method.

BMD analysis

A GLMM was applied for differential gene expression analysis, appropriate for count data with a negative binomial distribution and repeated measures. To align with the normal distribution assumption for dose-response modeling using BMDExpress, we modeled the $\log_2$-transformed CPM. Details on the modeling approach are provided in a previous study (Vuong et al. 2025).

The $\log_2$-transformed CPM values were filtered based on differential gene expression data, retaining probes with at least a 1.5-fold change and unadjusted p value <.05. These were read into BMDExpress v3 for BMD analysis, using a BMR of 50% and Bayesian model averaging for BMD estimation. Additional filtering, based on best practices and experience, excluded BMDs above the highest dose or with BMD/BMDL ratios exceeding 20 or BMDU/BMDL ratios greater than 40. A BMR of 50% was selected to balance sensitivity and robustness, avoiding over-interpretation of minor fluctuations and ensuring biologically relevant responses (Repetto et al. 2022; Pečinka et al. 2024; Yu et al. 2024).

A comparable approach was used for protein data, with modifications to enhance sensitivity to smaller fluctuations in protein levels. Normalized protein intensities were prefiltered using a 1.2-fold change threshold and an unadjusted Williams-Trend test p value <.05, while a BMR of 5% was applied for BMD estimation. These adjustments reflect the importance of detecting even small variations in protein levels, as such changes can have significant biological impacts.

K-means clustering and pathway enrichment analysis

K-means clustering was performed using the kmeans() function in R. The fold change values (relative to 0 Gy) were $\log_2$-transformed and scaled to ensure comparability across genes and doses. The dose-response curve for each cluster was computed by averaging fold change values across all genes at each dose. Multiple values of k were evaluated, with k = 11 selected for transcriptomic data and k = 6 for proteomic data. These values were chosen to balance the similarity of responses within clusters and the separation between them, while avoiding over-splitting or grouping biologically distinct patterns. Although some clusters appeared similar in shape, they were retained as distinct if they differed in key features such as response magnitude, directionality, inflection points, and stabilization behavior. Standard error of the mean expression was plotted for each dose.

Gene identifiers (Ensembl and gene symbols) from both transcriptomic and proteomic datasets were analyzed using Ingenuity Pathway Analysis (IPA; Qiagen), selecting the largest fold change for each gene or protein. IPA Core Analysis was performed with an expression threshold of ≥1.5 or ≤0.66 for transcriptomic data and ≥1.2 or ≤0.83 for proteomic data, with a significance cutoff of $p \leq .05$. Canonical pathways containing at least three genes or proteins were included in the analysis, and median pathway BMDL values were calculated as the median of the BMDLs of the constituent genes within each pathway.

Results

BMD modeling of transcriptomic and proteomic responses

WBCs, primarily lymphocytes, were isolated from the blood samples of 14 human donors. Isolated WBCs were exposed to X-ray radiation at doses ranging from 0.05 to 6 Gy at a rate of 0.05 Gy/min. Cytotoxic effects were evaluated 24 h post-exposure, measuring relative ATP levels, cell membrane integrity (TBE), and cell counts. The exposures caused a statistically significant, dose-dependent reduction in cellular ATP levels ($p < .05$), with minimal changes in cell membrane integrity, and cell counts remained unchanged (Supplementary Figure 1).

Transcriptomic and proteomic analysis of the irradiated WBCs revealed 1,204 genes and 168 proteins that conformed to BMD models. Subsequent analyses were based on BMDL values (Figure 1). The distribution of transcriptomic and proteomic BMDL values displayed a unimodal pattern. Transcriptomic BMDL values ranged from 0.001 to 4.6 Gy, peaking at 1.0–1.2 Gy (Figure 1(A)). A gradual decline in the number of responsive genes was observed beyond 1.2 Gy, with few genes responding above 4 Gy. Proteomic BMDL values ranged from 0.001 to 1.94 Gy, with a peak at 0.2 Gy and very few proteins exhibiting BMDL values above 0.7 Gy (Figure 1(B)). The median BMDL values were 1.38 Gy for genes and 0.21 Gy for proteins (Figure 1(C)).

Clustering of dose-response data

Dose-response data for BMD-modeled genes and proteins were grouped using k-means clustering to identify molecules that showed similar dose response patterns to radiation (Figure 2, Supplementary Table 1). This analysis revealed distinct response types, including dose-dependent upregulation and downregulation, low-dose hypersensitivity, and multi-phasic responses.

For transcriptomic data, k-values from 5 to 30 were tested, and 11 unique clusters were selected to balance heterogeneity without excessive repetition. Clusters C1, C3, and C4 exhibited rapid increases in gene expression at lower doses (up to 0.5 Gy), followed by a plateau or a gradual decline at higher doses (Figure 2(A)). Conversely, clusters C2 and C5 exhibited a rapid decrease in expression in response to lower doses after which expression stabilized.

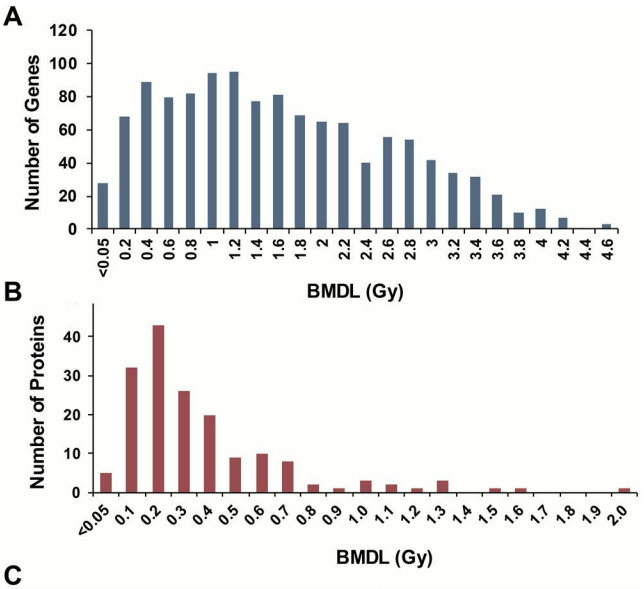

C

	No. of Targets	Median BMDL	Median BMD	Median BMDU
Genes	1204	1.38	3.05	6.03
Proteins	168	0.21	1.14	2.96

Figure 1. Summary of BMD modeling analysis. The histograms display the distribution of BMDL values and the associated number of (A) genes and (B) proteins. (C) Tabular summary of median BMDL, BMD, and BMDU values for transcriptomic and proteomic responses. BMD: benchmark dose; BMDL: BMD lower confidence limit; BMDU: BMD upper confidence limit.

Notably, C7 exhibited progressive downregulation, with a gradual but more pronounced decrease in expression at higher doses. Low dose hypersensitivity was observed in clusters C6, C8, C9 and C10, characterized by a sharp increase/decrease in gene expression, immediately followed by a rapid return to baseline. C1 was unique in that it displayed a bi-phasic response, with a rapid rise in expression up to 0.5 Gy and a gradual decrease thereafter.

For proteomic data, k-means clustering identified six optimal clusters (Figure 2(B)). Cluster C1 exhibited low dose hypersensitivity, with a sharp increase in protein expression at 0.05 Gy, returning to baseline by 0.1 Gy. Expression levels increased with dose in clusters C2, C3, and C4, with protein expression increasing at lower doses (up to 0.25 Gy) and plateauing thereafter. In contrast, clusters C5 and C6 demonstrated dose-dependent downregulation, with a steep decline in expression at lower doses (0.05–0.5 Gy) followed by stabilization beyond 2 Gy.

Pathway analysis of transcriptomic and proteomic responses

To gain insights into the biological significance of the BMD-modeled genes and proteins, differentially expressed targets were mapped to canonical pathways (Figure 3). Pathway analysis of genes fitting BMD models identified 335 significantly over-represented pathways, with most pathways exhibiting BMDL values between 0.6 Gy and 2 Gy, and a median pathway BMDL of 0.98 Gy (Figure 3(A,C)). For proteins, the BMDL distribution for pathways was shifted toward lower doses, with a prominent peak at approximately 0.2 Gy (Figure 3(B,C)). The majority of pathways in the proteomic analysis had median BMDLs below 0.4 Gy, and very few pathways were associated with BMDL medians above 0.6 Gy (Figure 3(B,C)).

The pathway analysis of genes fitting BMDs revealed over-representation of several key biological processes associated with radiation exposure, including DNA damage and repair, cell cycle regulation, cell death, cellular stress, lipid and glucose metabolism, and immune response (Table 1). Cancer-related pathways were also prominent, with median BMDL values of approximately 1 Gy. In contrast, proteomic pathway analysis identified processes predominantly linked to cellular stress, cytoskeletal dynamics, cell death, and immune response (Table 2). Notably, cytoskeletal regulation was a unique category in the proteomic data, whereas transcriptomic pathways were highlighted by DNA damage/repair, cell cycle regulation, and metabolic as well as cancer-related pathways.

Functional mapping of dose-response patterns

Next, genes and proteins from each functional category were mapped to the dose-response k-means clusters shown in Figure 2. The heatmap in Figure 4 depicts the percentage of genes within each functional category associated with each dose-response cluster, with the median BMDL of the cluster shown on the right y-axis. Transcriptomic pathways related to DNA damage/repair, cell cycle regulation, and cell death were predominantly in clusters exhibiting lower BMDL values (C1–C3) (Figures 4(A) and 5). Cellular stress and metabolic pathways displayed a broader distribution, having genes with both low median BMDLs (in C3) and high median BMDLs (in C11). Immune response and cancer development pathways were associated with a wide range of clusters but were particularly associated with clusters having higher median BMDLs (e.g. C7–C11), with the highest proportion of genes being assigned to C7 with a median BMDL of 1.28 Gy.

The association of proteomic pathways with dose-response clusters was less heterogeneous than the transcriptomic pathways (Figures 4(B) and 6). Proteins from all functional categories, cell death, cellular stress, cell movement, and immune response, had genes associated with clusters C3, C4, and C5, which had BMDL values ranging from 0.16 to 0.22 Gy. Interestingly, cluster C4 showed the highest association across all categories, whereas clusters C2 and C6 exhibited the lowest levels of association.

Discussion

The International Commission on Radiological Protection (ICRP) acknowledges significant uncertainty in the health effects of low-dose ionizing radiation, particularly regarding cancer risk (Laurier et al. 2021). This uncertainty stems from the challenge of detecting small risk increases against natural background variability in epidemiological

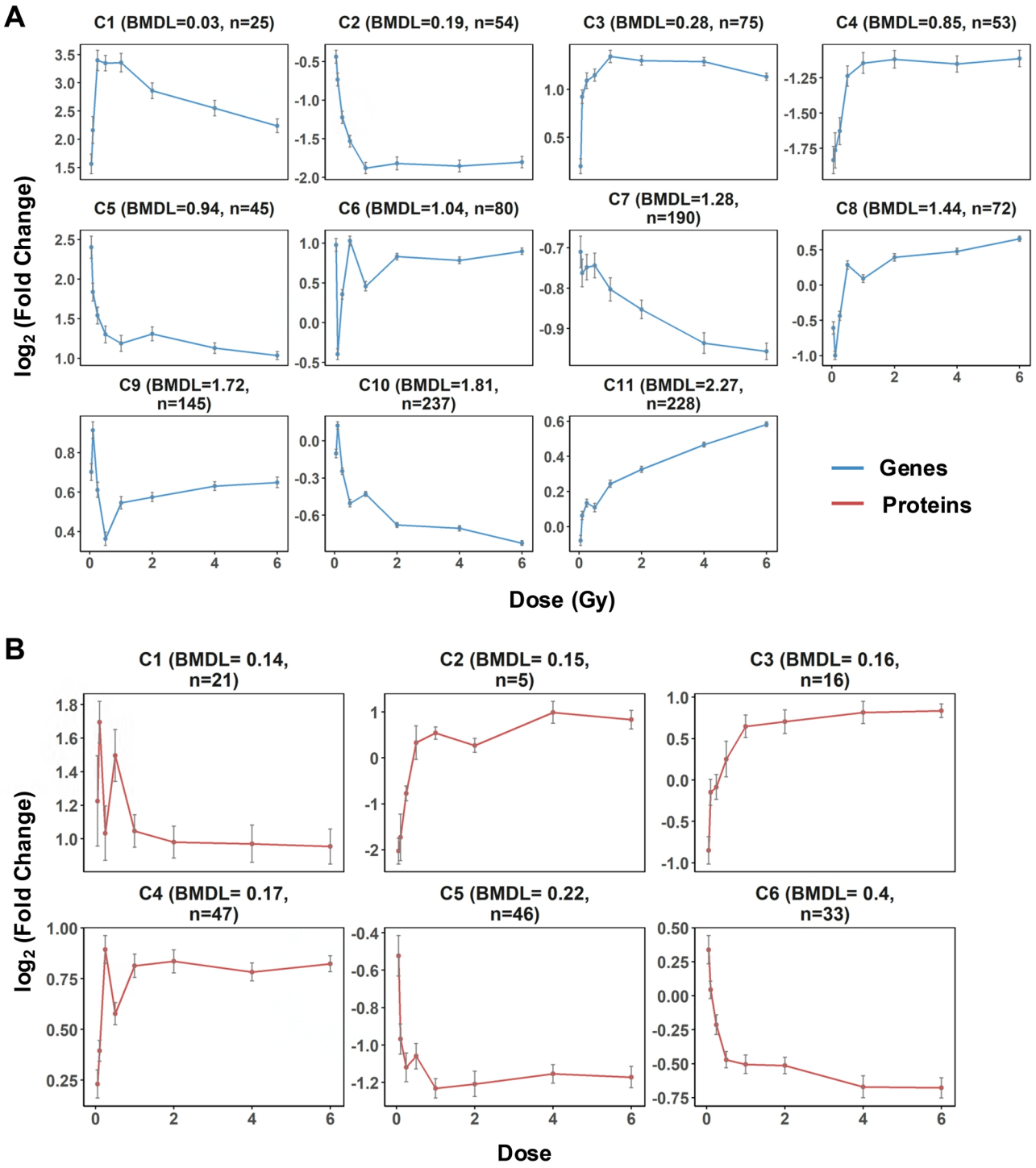

Figure 2. Dose-response clusters of BMD-modeled targets. K-means clustering was applied to the dose-response data (fold change relative to 0 Gy) for BMD-modeled (A) genes ($k = 11$) and (B) proteins ($k = 6$). The average dose-response curve for each cluster is shown, with the median cluster BMDL value and the number of genes/proteins in each cluster indicated above each panel. Clusters are ordered from lowest to highest median cluster BMDL. BMDL: BMD lower confidence limit.

studies, as well as compensatory mechanisms that mitigate radiation-induced damage (Mattsson and Nilsson 2015). These challenges complicate risk assessment and emphasize the need for molecular and mechanistic studies to refine our understanding of LDR effects. In this study, we examined molecular responses to LDR using k-means clustering to identify dose-response patterns and applied BMD modeling to determine the lowest dose of activity for genes and proteins as well as their associated pathways. Both the transcriptional and proteomic responses showed varying dose-response relationships including dose-dependent activation or repression, as well as multi-phasic trends and low dose hypersensitivity, with activity peaking between 0.05 and 0.25 Gy. These results suggest that gene and protein expression changes are sensitive indicators of cellular responses to LDR, though further validation will be needed to establish their functional relevance.

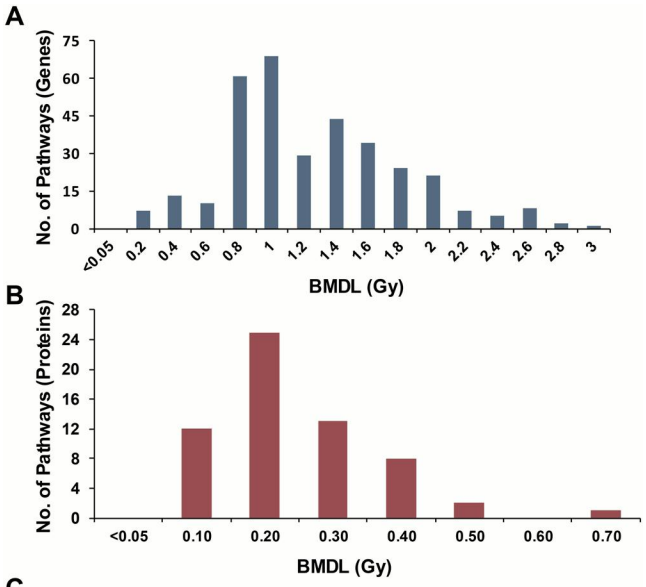

C

	No. of Targets	Median BMDL	Median BMD	Median BMDU
Genes	335	0.98	2.55	4.94
Proteins	61	0.17	0.97	2.64

Figure 3. Summary of pathway-based BMD metrics. Distribution of median pathway BMDLs for (A) genes and (B) proteins. (C) Tabular summary of median BMDL, BMD, and BMDU values for gene- and protein-based pathway analysis. BMD: benchmark dose; BMDL: BMD lower confidence limit; BMDU: BMD upper confidence limit.

BMD modeling identified 1,204 genes and 168 proteins showing a dose-response following radiation exposure. Transcriptomic BMDL values ranged from 0.001 Gy to 4.6 Gy, peaking at approximately 1.0–1.2 Gy. These findings corroborate prior transcriptomic studies that have reported substantial alterations in gene expression following radiation exposure to doses ranging from 0.005 Gy to 5 Gy (Nosel et al. 2013; Lee et al. 2014; Fang et al. 2022). Additionally, transcriptomic- and proteomic-based pathways displayed median BMDL values of 0.98 and 0.17 Gy, respectively. Lee et al. (2014) found that exposure to 1 Gy of radiation significantly altered gene expression, particularly in pathways related to DNA damage repair, cell cycle regulation, and apoptosis in peripheral blood mononuclear cells (Nosel et al. 2013; Lee et al. 2014; Fang et al. 2022). The authors hypothesized that 1 Gy may be a critical point at which major biological changes begin to occur. Although the median BMDL for transcriptomic pathways from our study (0.98 Gy) supports this observation, pathways associated with cell death, cell cycle regulation, and DNA damage were activated at much lower doses, with the lowest BMDL values in each category falling below 0.5 Gy, consistent with findings from a previous study conducted at a dose rate of 1 Gy/min (Vuong et al. 2025).

Although this study applied BMD modeling to analyze radiation-induced molecular responses similar to Vuong et al. (2025), the latter study applied BMD modeling within the context of the AOP framework, using transcriptomic and proteomic data to establish mechanistic evidence for radiation effects with a high dose rate (1 Gy/min) typical of acute exposures. In contrast, the current work focuses specifically on characterizing the dose-response behavior of gene and protein expression profiles at a lower dose rate of 0.05 Gy/min, more relevant to environmental and occupational settings. The observed similarity in pathway-level BMD analysis between the studies was not expected and may point to a level of robustness in radiation-responsive pathways. However, a direct, dose-by-dose comparison across dose rates is needed to evaluate potential dose-rate effects.

Clustering of BMD-modeled gene and protein dose-response profiles identified distinct expression patterns, indicative of diverse molecular responses to radiation exposure. DNA damage-related genes were primarily associated with clusters C3, C11, and C1, all showing an increase in gene expression up to 1 Gy. Genes with BMDL <0.1 Gy, including *POLH, MDM2, GADD45A, BBC3, TNFRSF10B, and BAX*, were among the earliest to respond, suggesting that even small doses of radiation exposures can initiate DNA damage response pathways (Amundson et al. 2003; Lacombe et al. 2018). Genes in C11 showed a continued increase in expression at higher doses, potentially indicating responses to persistent or escalating cellular stress. For instance, this cluster included genes such as H2AJ, which is associated with persistent DNA damage and senescence, and genes involved in H2B ubiquitination, a process that facilitates DNA repair (Giannattasio et al. 2005; Isermann et al. 2020).

Genes involved in cell cycle regulation were predominantly found in C7, C3, C1, and C10, with BMDL values ranging from 0.03 to 1.81 Gy. C1 included genes that were associated to DNA repair, whereas C3 exhibited increased expression of cell cycle regulators such as *PLK3*, *CDKN1A*, *PPM1D*, and *PCNA* starting at low doses, which may reflect activation of cell cycle checkpoints in response to DNA damage (Xie et al. 2001). Interestingly, cell cycle regulators in C7 and C10 (*CDKN2D*) exhibited decreased expression at doses >0.5 Gy, suggesting suppression of cell cycle regulators at higher doses. Together, these patterns suggest that low-dose radiation may promote checkpoint activation and repair, whereas higher doses could shift the balance toward cell cycle inhibition in response to more extensive damage (Xie et al. 2001; Cazzalini et al. 2010; Shaltiel et al. 2015).

Cell death, cellular stress, and metabolic pathways were associated with clusters C3, C9, and C11. Genes in C3 (*HSPA1B, CDKN1A, BCL2L1, AHC1, UBB, and TIGAR*) showed increased expression at low doses and were associated with pathways such as heat shock response, MAPK signaling, and redox homeostasis, suggesting activation of stress adaptation mechanisms. In contrast, C9 was characterized by low-dose hypersensitivity and was associated with oxidative stress, inflammation, and apoptotic signaling. Proteomic data supported these trends, showing involvement of mitochondrial and pro-apoptotic proteins showing increased expression at higher doses across multiple clusters (C2, C3, C4). Collectively, these patterns may reflect a progression from stress adaptation to apoptosis with increasing dose. Interestingly, the enrichment of transcriptomic and

Table 1. Pathway analysis of transcriptomic data.

Canonical pathways	Median BMDL	Genes
DNA damage and repair		
p53 signaling	0.20	*POLH, MDM2, GADD45A, BBC3, TNFRSF10B, BAX, UBB, H2BC11, FAS, TIGAR, H1-1, H2AX, H2BC26, CDKN1A, MYC, PPM1D, PCNA, GADD45G, DRAM1, CCNG1, CABIN1, H2BC5, GADD45B, MAPK11, H2AJ, H2BC3, H2BC13, H2AC7, JUN, H1-2, H2AC14, POLD2, RRM2B, SMAD4, H2BC17, TGFB1, TP53INP1, TP53I3, SUV39H1, H1-5, PPP2R1A, PALB2, PPP2R5C, PPP5C, APBB1, H1-4, CDKN1B, TERF1*
GADD45 signaling	0.22	
HDR through homologous recombination or single strand annealing	0.27	
Nonhomologous end-joining (NHEJ)	0.34	
ATM signaling	0.35	
DNA double strand break response	0.51	
DNA damage/telomere stress induced senescence	0.70	
Cell cycle regulation		
TP53 regulates transcription of cell cycle genes	0.17	*MDM2, GADD45A, BAX, PLK3, PLK2, CDKN1A, MYC, PPM1D, PCNA, E2F5, CDKN2D, RBL2, CDKN2C, SMAD4, KLF4, TGFB1, SUV39H1, HDAC7, CDC25B, BTG2, YWHAQ, CDKN1B*
Cell cycle: G2/M DNA damage checkpoint regulation	0.18	
Cell cycle: G1/S checkpoint regulation	0.99	
FOXO-mediated transcription of cell cycle genes	1.02	
Cell death		
MYC mediated apoptosis signaling	0.12	*MDM2, BBC3, TNFRSF10B, GLS2, BAX, HSPA2, UBB, GZMA, FAS, GZMB, H2AX, HSPA1B, FASLG, H2BC26, CDKN1A, MYC, GZMH, PRF1, GZMM, RASD1, H2BC5, BCL2L11, ADRB2, ABCA1, CGAS, RBL2, H2AC21, HMOX1, GZMK, LPCAT3, GSS, ATG12, FTH1, FLOT2, STEAP3, DAPK1, H2BC17, CTSB, SLC7A11, MRAS, LRP1, SDCBP, RALB, H2AC18, SREBF2, SLC38A1, H2AC19, FPR1, NFE2L2, CYBB, DDIT3, HSPA5*
RIPK1-mediated regulated necrosis	0.12	
FOXO-mediated transcription of cell death genes	0.25	
Immunogenic cell death signaling pathway	0.49	
Ferroptosis signaling pathway	1.09	
Cell stress		
Oncogene induced senescence	0.46	*MDM2, HSPA2, UBB, H2BC11, MAP4K4, H2AX, HSPA1B, H2BC26, CDKN1A, ID1, ACTA2, RASD1, H2BC5, SIRPA, PRKCH, CDKN2D, MAPK11, PPARG, NQO1, H2AJ, H2BC3, CXCL8, H2BC13, HMOX1, H2AC7, DNAJA4, PPP1R15A, CEBPB, FOS, JUN, H2AC14, RHOB, SREBF1, FTH1, ARG2, CDKN2C, H2BC17, APOC1, SLC7A11, APOE, RHOU, RHOH, MRAS, SOD2, MAFF, PPP2R1A, RALB, VENTX, SREBF2, ETS1, NCF2, NCF1, PPP2R5C, SRC, NFE2L2, ETS2, CYP2S1, PRKCB, S100A8, CYBB, JUNB, DDIT3, DNAJB11, AKR1A1, MAFG, DNAJA3, CDKN1B, HSPA5*
Oxidative stress induced senescence	0.59	
Senescence-associated secretory phenotype (SASP)	0.72	
UVC-induced MAPK signaling	0.98	
Unfolded protein response	1.14	
NFE2L2 regulating anti-oxidant/detoxification enzymes	1.14	
Production of nitric oxide and ROS in macrophages	1.60	
NRF2-mediated oxidative stress response	1.78	
Lipid and glucose metabolism		
TP53 regulates metabolic genes	0.71	*TNFSF8, TNFSF4, CD70, GLS2, DDIT4, TIGAR, MAP4K4, FASLG, PDGFD, RASD1, PTGS2, IL18RAP, TNFSF9, PPARG, RRAGD, NQO1, ABCA1, CCL2, CXCL8, CYP27A1, HMOX1, SESN2, FOS, LTB, JUN, SESN1, SREBF1, RRM2B, TNFSF15, ARG2, APOC1, TGFB1, HK2, GLA, ABCG1, APOE, DHCR24, NEU1, MRAS, CD14, RALB, OSM, SC5D, YWHAQ, SREBF2, CTSA, SRA1, SPHK1, HK3, MMP9, ALDH3B1, CERS6, SRC, NFE2L2, S100A8, HK1, IDI1, ARSA, ESYT1, TXNIP, INSR, DDIT3, HEXB, NR1H3, MAFG, SUMF1*
PPAR signaling	0.89	
FXR/RXR activation	0.93	
LXR/RXR activation	1.41	
Cholesterol biosynthesis	2.11	
Glucose and glucose-1-phosphate degradation	2.48	
Sphingolipid metabolism	2.62	
Immune response		
Differential regulation of cytokine production in macrophages and T helper cells	0.39	*TNFSF8, CX3CR1, TNFSF4, TNFRSF10B, CD70, ADGRG1, BAX, HSPA2, NMUR1, UBB, FAS, NCR3, XCL1, EOMES, MAP4K4, KLRD1, GZMB, HSPA1B, FASLG, TRDC, CDKN1A, NCR1, TRGV9, KIR2DL1, MYC, IGHM, ACTA2, IL12RB2, PRF1, CCL5, TRDV2, JCHAIN, GPR153, CCL4, CD244, RASD1, KLRB1, TBX21, IL10, PRKCH, XCL2, ARHGAP6, IL18RAP, TGFBR3, MMP23B, KLRC3, PTGDR, ITPR2, TRGC2, CXCL2, MAPK11, CCL18, IL2RB, TNFSF9, IL23A, HCAR2, ELMO1, FCAR, TLR9, TLR10, ADRB2, KLRC2, TRGC1, GPR18, HAVCR2, CGAS, CCL2, ITGB7, GAB2, CXCL8, KLRK1, TRAV26-2, ADGRA2, PLA2G7, IL2RG, CD247, CCR6, HMOX1, TIMP3, BHLHE41, IGLC3, P2RY10, PTAFR, FOS, CCRL2, AIM2, LTB, CCR1, COL4A4, JUN, TRBC1, ICAM3, CXCL1, CHD4, TXK, SELPLG, FTH1, KLRC4, TNFSF15, CLDN15, LAG3, PLA2G4C, CARD11, ADGRE2, BTLA, CD80, IL18R1, DOCK1, TGFB1, LCK, SIGIRR, MMP14, CSF2RA, TRGV4, LTBR, NLRC3, TRBV30, CD40, NLRC4, IRAK3, NFATC2, TRBV12-4, RHOH, MRAS, CCL24, HCST, TRBV19, HCK, CCR7, ARPC5L, TRBV5-1, FPR3, LPAR6, PPP2R1A, ATP6V0D1, RALB, GPR183, OSM, TRBV14, ITGAX, NCF2, IRAK1, TRBV29-1, PIP4K2A, NCF1, PPP2R5C, SPHK1, MMP9, TRBV6-2, IL21R, TRBV27, FPR1, NECTIN2, GPR174, SRC, CD83, CCL3L1, PRKCB, PLAAT4, S1PR4, CYBB, GPR162, JUNB, PLD3, CIITA, GNAQ, INSR, TLR5, ITGAV, PRDM1, S1PR2, CD3E, STX11, FCER1G, HSPA5, ATP6V1B2*
Natural killer cell signaling	0.51	
Pathogen induced cytokine storm signaling pathway	0.70	
CGAS-STING signaling pathway	0.70	
Crosstalk between dendritic cells and natural killer cells	0.75	
Th1 and Th2 activation pathway	0.81	
Macrophage classical activation signaling pathway	0.93	
Toll-like receptor signaling	0.93	
Chemokine signaling	0.98	
Phagosome formation	1.09	
Leukocyte extravasation signaling	1.18	
T cell exhaustion signaling pathway	1.33	
NF-κB signaling	1.54	
Cancer		
Tumor microenvironment pathway	0.72	*MDM2, BBC3, CX3CR1, ADGRG1, BAX, NMUR1, TRIB2, FAS, FASLG, CDKN1A, ID1, MYC, HHAT, IL12RB2, ARHGEF3, PDGFD, GPR153, RASD1, BCL2L11, PTGS2, IL10, PRKCH, E2F5, IL18RAP, CDKN2D, TGFBR3, MMP23B, PTGDR, HBEGF, MAPK11, IL2RB, HCAR2, PLAUR, ADRB2, LRP5, GPR18, CCL2, ITGB7, GAB2, CXCL8, RBL2, ADGRA2, IL2RG, CCR6, P2RY10, ARHGEF6, PTAFR, FOS, CCRL2, CCR1, EGR1, JUN, CXCL1, RHOB, BLK, CDKN2C, TCF3, SMAD4, ADGRE2, KLF4, SPP1, IL18R1, AXIN1, TGFB1, LCK, MMP14, PLCD1, SUV39H1, NFATC2, RHOU, RHOH, MRAS, LRP1, HDAC7, HCK, CCR7, FPR3, LPAR6, PPP2R1A, RALB, GPR183, CDC25B, OSM, YWHAQ, ITGAX, ETS1, PPP2R5C, MMP9, IL21R, FPR1, ARHGEF1, GPR174, SRC, ETS2, PRKCB, S1PR4, GPR162, GNAQ, ITGAV, S1PR2*
Molecular mechanisms of cancer	0.89	
Role of tissue factor in cancer	1.12	
MSP-RON signaling in cancer cells pathway	1.28	
Chronic myeloid leukemia signaling	1.29	

proteomic cell death pathways was not accompanied by a measurable decrease in cell number or loss of membrane integrity (Supplementary Figure 1). This suggests that molecular indicators of cell death may precede overt cytotoxicity, emphasizing the importance of examining cellular responses beyond the initial 24 h.

Immune-related and cancer-associated genes exhibited diverse dose-response patterns following radiation exposure.

Table 2. Pathway analysis of proteomic data.

Ingenuity canonical pathways	Median BMDL	Proteins
Cell death		
Death receptor signaling	0.11	CYBB, HSPB1, LMNA, ARHGDIB, CYC1, VDAC3, SLC25A6, SLC25A5, VDAC2, FTL
Ferroptosis signaling pathway	0.33	
Necroptosis signaling pathway	0.35	
Cell stress		
ERK/MAPK signaling	0.18	CYBB, PSMB9, ITGA2B, HSP90B1, ITGB3, HSPB1, COX4I1, HK1, UBE2V1, UQCR10,
Protein ubiquitination pathway	0.21	SDHA, CYC1, VDAC3, ITGAM, ATP5F1C, FUS, PARK7, UBE2N, TLN1, NCF2, GPX1,
Mitochondrial dysfunction	0.29	PSME1, SRC, ATP5PO, VDAC2, LDHB, COPS5, PSMA2, USP9X
HIF1α signaling	0.31	
Cell structure and movement		
Regulation of actin-based motility by rho	0.08	ITGA2B, GSN, ITGB3, VCL, FLNA, EZR, ITGAM, CAST, TLN1, PFN1, SRC
Actin cytoskeleton signaling	0.17	
Regulation of cellular mechanics by calpain protease	0.22	
Immune response		
Antigen presentation pathway	0.11	CYBB, FGA, CTSG, PSMB9, ITGB3, VCL, HLA-DRB3, SDHA, CYC1, CANX, H1-0,
Macrophage classical activation signaling pathway	0.13	MPO, EZR, SYK, VDAC3, STXBP2, LTF, ITGAM, RAB27A, ATP5F1C, NCF2, ELANE,
Phagosome maturation	0.16	SLC25A6, SLC25A5, SPN, SELP, ATP6V1A, SRC, VDAC2, TUBB1, H1-5, SET,
IL-8 signaling	0.22	UNC13D, FTL
Pathogen induced cytokine storm signaling pathway	0.22	
Leukocyte extravasation signaling	0.27	
Neutrophil extracellular trap signaling pathway	0.27	
Granzyme A signaling	0.60	

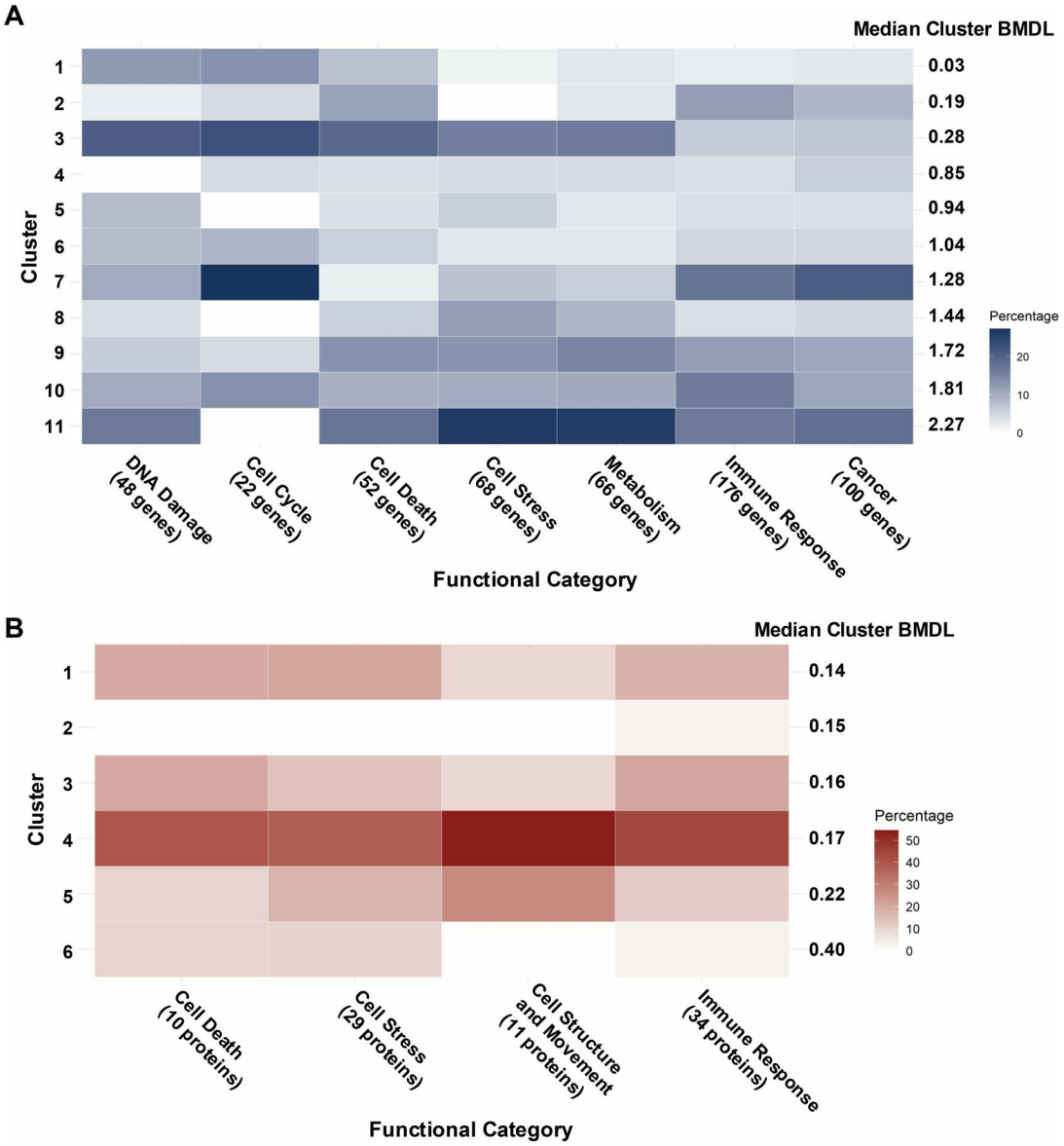

Figure 4. Functional mapping of dose-response patterns. Heatmaps display the percentage of (A) genes and (B) proteins from each functional category that are associated with each dose-response cluster from Figure 2. The median cluster BMDL value is provided to the right of each heatmap. BMDL: BMD lower confidence limit.

Functional Category	Enriched Clusters	Dose-Response Curve	Low (<0.1Gy)	Medium (0.1 - 1Gy)	High (> 1Gy)
DNA Damage	C3		UBB, TIGAR	H2BC26, CDKN1A, PPM1D, PCNA, DRAM1, CCNG1, H2BC5	H2AC14
	C11			H2BC5, H2AJ, H2BC3, JUN	H1-2, H2AC14, H2BC17, H1-5, PALB2, H1-4
	C1		POLH, MDM2, GADD45A, BBC3, TNFRSF10B, BAX		
Cell Cycle	C7			CDKN2D	CDKN2C, SMAD4, TGFB1, SUV39H1, YWHAQ
	C3		PLK3	CDKN1A, PPM1D, PCNA	KLF4
	C1 ; C10	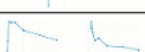	C1 - MDM2, GADD45A, BAX		C10 - HDAC7, CDC25B, CDKN1B
Cell Death	C3		GLS2, UBB	HSPA1B, H2BC26, CDKN1A, RASD1, H2BC5, BCL2L11, ABCA1	FTH1
	C9			HMOX1, LPCAT3	GSS, STEAP3, DAPK1, CTSB, CYBB
	C11			CGAS, H2AC21	H2BC17, SDCBP, H2AC18, H2AC19, FPR1, DDIT3, HSPA5
Cell Stress	C11			H2AJ, H2BC3, CEBPB, JUN	RHOB, H2BC17, APOC1, RHOU, VENTX, NCF2, SRC, ETS2, CYP2S1, JUNB, DDIT3, DNAJB11, AKR1A1, HSPA5
	C3		UBB	MAP4K4, HSPA1B, H2BC26, CDKN1A, ID1, RASD1, H2BC5, SIRPA	H2AC14, FTH1
	C9			NQO1, CXCL8, HMOX1, H2AC7, FOS	APOE, NCF1, S100A8, CYBB
Metabolism	C11			CYP27A1, SESN2, JUN	APOC1, HK2, CTSA, SPHK1, HK3, CERS6, SRC, HK1, ARSA, INSR, DDIT3, HEXB, NR1H3, SUMF1
	C3		CD70, GLS2, DDIT4, TIGAR	MAP4K4, RASD1, PTGS2, TNFSF9, RRAGD, ABCA1, CCL2	
	C9			NQO1, CXCL8, HMOX1, FOS	APOE, NEU1, CD14, MMP9, ALDH3B1, S100A8
Immune Response	C7			IL12RB2, JCHAIN, GPR153, CCL4, PRKCH, TRGC2, TLR9, TLR10, KLRC2, ITGB7, TRAV26-2, CD247, CCR6, IGLC3, P2RY10, AIM2	ICAM3, KLRC4, CLDN15, CARD11, BTLA, TGFB1, TRGV4, NLRC3, CD40, NFATC2, TRBV12-4, TRBV5-1, PRKCB, PLAAT4, S1PR4
	C10			IGHM, XCL2, KLRC3, TRGC1, GPR18, KLRK1, IL2RG, LTB, TRBC1	CHD4, TXK, LAG3, LCK, SIGIRR, TRBV30, RHOH, MRAS, HCST, TRBV19, ARPC5L, PPP2R1A, TRBV14, TRBV29-1, PIP4K2A, PPP2R5C, TRBV6-2, TRBV27, GPR174, CD3E
	C11			IL23A, HAVCR2, CGAS, PTAFR, JUN	MMP14, IRAK3, HCK, ATP6V0D1, ITGAX, NCF2, SPHK1, IL21R, FPR1, SRC, CD83, CCL3L1, GPR162, JUNB, PLD3, CIITA, GNAQ, INSR, ITGAV, S1PR2, STX11, FCER1G, HSPA5, ATP6V1B2
Cancer	C7			IL12RB2, PDGFD, GPR153, PRKCH, CDKN2D, ITGB7, CCR6, P2RY10	BLK, CDKN2C, TCF3, SMAD4, AXIN1, TGFB1, SUV39H1, NFATC2, YWHAQ, ETS1, ARHGEF1, PRKCB, S1PR4
	C11				BLK, CDKN2C, TCF3, SMAD4, AXIN1, TGFB1, SUV39H1, NFATC2, YWHAQ, ETS1, ARHGEF1, PRKCB, S1PR4
	C9; C10			C9 - ARHGEF3, HCAR2, PLAUR, CXCL8, FOS, CCR1 C10 - GPR18, IL2RG	C9 - CXCL1, CCR7, FPR3, GPR183, MMP9 C10 - LCK, PLCD1, RHOH, MRAS, HDAC7, PPP2R1A, CDC25B, PPP2R5C, GPR174

Figure 5. Top enriched dose-response gene clusters across functional categories. The top three dose-response clusters with the highest percentage of gene association from each functional category, with genes classified by low, medium, and high BMDL values.

Genes in C10 (IGHM, XCL2, KLRC3, TLR3) showed increased expression at doses up to 0.1 Gy, similar to increased expression of proteins in clusters C4, C3, and C1. In contrast, distinct transcriptomic profiles were observed at higher doses (>1 Gy): suppression of C7 genes (*IL12RB2, JCHAIN, TLR4*) suggests a downregulation of immune activation, potentially to limit excessive inflammation, while elevated expression of C11 genes (*IL23A, CGAS, JUN*) may reflect dose-dependent inflammatory signaling. Cancer-related genes also demonstrated varying dose-response trends. Genes in C7 (*PDGFD, PRKCH, CCR6*) showed reduced expression at higher doses of pro-tumorigenic targets, while genes in C9 and C10 (*ARHGEF3, CXCL8, FOS, CCR1, GPR18, IL2RG, LCK*) exhibited low-dose hypersensitivity with enrichment for angiogenesis, inflammatory signaling, and cell migration pathways. These patterns reflect dose-dependent changes in immune and cancer-related gene expression, but the functional significance of these observations remains to be confirmed (Bogdándi et al. 2010; Cui et al. 2017; Karimi et al. 2017).

In interpreting pathway-level responses from BMD modeling, it is important to consider that genes may contribute to multiple pathways and that contributions of constituent genes within a pathway differ. Some genes may be functionally redundant or act downstream of primary regulators, potentially leading to complex or overlapping pathway signals. However, BMD modeling is not influenced by pathway exclusivity; it fits a dose-response curve to each gene independently, estimating the dose at which a predefined level of change occurs. As the BMD estimates are derived from the lower portion of the response curve, the method is sensitive to early molecular changes even when the full dynamic range of fold changes is not large. For instance, in our data, *UBB* and IL12RB2 showed low BMDL values (<0.3 Gy) but only modest changes in expression, consistent with their involvement in cellular stress response and immune signaling. In contrast, *DLG1* and *CXCR5* exhibited larger fold changes (>3-fold) but only at higher doses (BMDL >1.5 Gy), indicating secondary or downstream effects. This demonstrates that low-dose sensitivity, as captured by BMD, does

Functional Category	Enriched Clusters	Dose-Response Curve	Low (<0.1Gy)	Medium (0.1 - 1Gy)
Cell Death	C4		LMNA	SLC25A6, SLC25A5, VDAC2
	C1		HSPB1	VDAC3
	C3		CYBB	CYC1
Cell Stress	C4		HSP90B1	HK1, UQCR10, ITGAM, ATP5F1C, TLN1, NCF2, SRC, ATP5PO, VDAC2, USP9X
	C1		ITGA2B, HSPB1	SDHA, VDAC3, GPX1, PSMA2
	C5		PSMB9	UBE2V1, FUS, PARK7, PSME1
Cell Movement	C4		GSN	VCL, FLNA, ITGAM, TLN1, SRC
	C5			EZR, CAST, PFN1
	C1; C3		C1 - ITGA2B; C3 - ITGB3	
Immune Response	C4		CTSG	VCL, HLA-DRB3, H1-0, MPO, SYK, STXBP2, ITGAM, ATP5F1C, NCF2, ELANE, SLC25A6, SLC25A5, SRC, VDAC2
	C3		CYBB, FGA, ITGB3	CYC1, LTF, SELP, H1-5
	C1			SDHA, VDAC3, RAB27A, ATP6V1A, TUBB1, UNC13D

Figure 6. Top enriched dose-response protein clusters across functional categories. The top three dose-response clusters with the highest percentage of protein association from each functional category, with proteins classified by low, medium, and high BMDL values.

not necessarily correlate with the amplitude of expression and highlights the value of BMD modeling in identifying biologically relevant early responders. Nevertheless, we acknowledge that summarizing pathway BMDs using unweighted medians may obscure distinctions between early regulators and late responders, and future approaches could benefit from incorporating functional or network-based weighting.

Furthermore, while our study provides insights into the molecular profiles associated with LDR, the use of isolated lymphocytes, though controlled, may not fully reflect the complexity of tissue-specific responses or intercellular interactions observed in vivo. Additionally, this study assessed molecular responses at a single timepoint, limiting insight into temporal dynamics. Future studies with multiple timepoints are needed to distinguish between transient, delayed or persistent responses. These studies should also incorporate larger, more diverse donor populations to enhance the generalizability of these findings. Such efforts would account for individual variability in radiation sensitivity influenced by factors such as age, sex, genetic predisposition, and lifestyle (Zyla et al. 2014; Schmitz-Feuerhake et al. 2016; Narendran et al. 2019).

The LNT model has been a cornerstone in radiation protection for over 60 years. While more recent studies support its use in cancer risk assessment (Shore et al. 2019; Laurier et al. 2023), critics argue that it may be overly conservative (Kuikka 2009; Reed 2024). Radiobiological evidence challenges the assumption of a strictly linear dose-response, revealing hyper-radiosensitivity below 0.3 Gy and increased radioresistance at 0.4–1 Gy (Marples and Joiner 1993; Gamble et al. 2000; Joiner et al. 2001; Bahia et al. 2018; Koryakina et al. 2022). This study contributes to this body of evidence demonstrating complex, non-linear dose-response relationships using transcriptomic and proteomic analyses with exponential, biphasic, and hypersensitive responses peaking between 0.05 and 0.5 Gy. The ability to associate these patterns with specific doses through BMD modeling highlights the method's utility in mechanistic dose-response evaluation. These findings demonstrate that even low doses can elicit significant cellular responses that cannot be extrapolated from higher-dose data, emphasizing the need for a more mechanistic-based approach to radiation risk assessment.

Disclosure statement

No potential conflict of interest was reported by the author(s).

Funding

The project is funded by the Genomics Research and Development Initiative awarded to VC. The authors received the funding from the Pilot Mass Spectrometry Collaboration Center by Laboratories Canada.

Notes on contributors

Saadia Khilji is a Postdoctoral Fellow at the Radiation Protection Bureau of Health Canada and holds a Ph.D. in Cellular and Molecular Medicine with a specialization in Pathology and Laboratory Medicine from the University of Ottawa. Since joining the RPB in 2021, she has leveraged her expertise in systems biology, omics data, and computational biology to advance research in the field.

Ngoc Q. Vuong is a Senior Research Assistant at the Radiation Protection Bureau (RPB) of Health Canada. He graduated from the University of Ottawa with a Ph.D. degree in Biochemistry (specialized in environmental toxicology). He joined the RPB in 2018 and has expertise in areas of computational biology, bioinformatics, proteomics and high throughput assays.

Andrew Williams received an MSc in statistics from Carleton University, Ottawa, Ontario. Mr. Williams joined the Biostatistics Unit in the Environmental Health Science and Research Bureau at Health Canada in 2001. Mr. Williams has a broad knowledge of statistical theory and methods, with 23 years of experience working on projects requiring expertise in the areas of statistical inference, experimental design, generalized linear and generalized mixed modeling, and predictive modeling including data mining or machine learning methodologies.

Kelly M. Fulton is a research scientist in the Human Health Therapeutics Research Center at the National Research Council Canada. She holds a Ph.D. in Chemistry with a specialization in Biochemistry from Carleton University. She has broad analytical chemistry expertise in proteomics and mass spectrometry, and has led multiple projects focused on human health.

Isabel Baay holds a B.Sc. in Biochemistry with a Specialization in Microbiology and Immunology from the University of Ottawa. She worked as a technical officer in the Human Health Therapeutics Research Center at the National Research Council Canada, funded by Laboratories Canada to support projects associated with the Pilot Mass Spectrometry Collaboration Center.

Susan M. Twine is Director General of the Human Health Therapeutics Research Center at the National Research Council Canada. She obtained a Ph.D. in Biochemistry from the University of Southampton (UK). She joined the National Research Council in 2002, focusing on applications of mass spectrometry to address a variety of human health challenges. Dr. Twine is adjunct professor at Carleton University and is actively engaged in student mentoring.

Matthew J. Meier is a Research Scientist in the Mechanistic Studies Division in the Environmental Health Science and Research Bureau at Health Canada. His research involves the use of toxicogenomic methods for understanding the health effects of chemicals, with a focus on in vitro methods with the goal of reducing animal testing. His main interest is in developing reproducible computational/bioinformatic workflows for regulatory applications of genomics.

Premkumari Kumarathasan is a Research Scientist and is the Lead PI of the Analytical Biochemistry and Proteomics Laboratory in the Mechanistic Studies Division, Environmental Health Science and Research Bureau at Health Canada. She also holds an adjunct professor position at University of Ottawa. Her research focus is on the identification of toxicity mechanisms underlying environmental exposure-related adverse health effects through development & application of advanced biomarker approaches to support health risk analysis. Her research involves in vitro cell culture, in vivo animal models and human exposure studies. She applies targeted and untargeted OMIC (proteomics and metabolomics) biomarker analyses in her research work to identify toxicity pathways underlying environmental exposure-mediated adverse health outcomes.

Ruth C. Wilkins is a Research Scientist at the Consumer and Clinical Radiation Protection Bureau of Health Canada and the Manager of the Ionizing Radiation Health Sciences Division. She graduated with a Ph.D. in Medical Physics from Carleton University and has been employed at Health Canada since 1996. She is an Adjunct Professor and lecturer of Radiobiology in the Department of Physics at Carleton University and is on the Canadian delegation to the United Nations Scientific Committee on the Effects of Atomic Radiation (UNSCEAR).

Carole L. Yauk was the lead scientist of the Genomics Laboratory in the Environmental Health Science and Research Bureau at Health Canada for 18 years. She joined the University of Ottawa's Department of Biology as a professor in September 2020, where she holds the Canada Research Chair in Genomics and the Environment. Her research focuses on the development and implementation of genomic tools for human health risk assessment of environmental exposures. She is actively involved in various international committees to advance these fields.

Vinita Chauhan is a senior research Scientist at the Consumer and Clinical Radiation Protection Bureau of Health Canada. Her research focus includes application of new approach technologies to help reduce the uncertainty in health risks at low dose and low dose-rate radiation exposures. She is a Canadian delegate of the Nuclear Energy Agency High-Level Group on Low-Dose Research (HLG-LDR) and co-chairs an international Rad/Chem AOP Joint Topical Group which is working to integrate the use of adverse outcome pathways in radiation research.

ORCID

Saadia Khilji http://orcid.org/0009-0001-0188-6240
Ruth C. Wilkins http://orcid.org/0000-0002-9621-477X
Vinita Chauhan http://orcid.org/0000-0002-4498-0915

References

Amundson SA, Lee RA, Koch-Paiz CA, Bittner ML, Meltzer P, Trent JM, Fornace AJ. 2003. Differential responses of stress genes to low dose-rate gamma irradiation. Mol Cancer Res. 1(6):445–452. https://pubmed.ncbi.nlm.nih.gov/12692264/.

Bahia S, Blais E, Murugkar S, Chauhan V, Kumarathasan P. 2018. Oxidative and nitrative stress-related changes in human lens epithelial cells following exposure to X-rays. Int J Radiat Biol. 94(4):366–373. doi:10.1080/09553002.2018.1439194.

Bates D, Mächler M, Bolker B, Walker S. 2015. Fitting linear mixed-effects models Usinglme4. J Stat Soft. 67(1):1. doi:10.18637/jss.v067.i01.

Bogdándi EN, Balogh A, Felgyinszki N, Szatmári T, Persa E, Hildebrandt G, Sáfrány G, Lumniczky K. 2010. Effects of low-dose radiation on the immune system of mice after total-body irradiation. Radiat Res. 174(4):480–489. doi:10.1667/RR2160.1.

Boice JD. 2017. The linear nonthreshold (LNT) model as used in radiation protection: an NCRP update. Int J Radiat Biol. 93(10):1079–1092. doi:10.1080/09553002.2017.1328750.

Böyum A. 1968. Isolation of mononuclear cells and granulocytes from human blood. Isolation of monuclear cells by one centrifugation, and of granulocytes by combining centrifugation and sedimentation at 1 g. Scand J Clin Lab Invest Suppl. 97:77–89.

Cardarelli JJ, Ulsh BA. 2018. It is time to move beyond the linear no-threshold theory for low-dose radiation protection. Dose Response. 16(3):1559325818779651. doi:10.1177/1559325818779651.

Cazzalini O, Scovassi AI, Savio M, Stivala LA, Prosperi E. 2010. Multiple roles of the cell cycle inhibitor p21(CDKN1A) in the DNA damage response. Mutat Res. 704(1-3):12–20. doi:10.1016/j.mrrev.2010.01.009.

Chauhan V, Hamada N, Monceau V, Ebrahimian T, Adam N, Wilkins RC, Sebastian S, Patel ZS, Huff JL, Simonetto C, et al. 2021. Expert consultation is vital for adverse outcome pathway development: a case example of cardiovascular effects of ionizing radiation. Int J Radiat Biol. 97(11):1516–1525. doi:10.1080/09553002.2021.1969466.

Chauhan V, Rowan-Carroll A, Gagné R, Kuo B, Williams A, Yauk CL. 2019. The use of in vitro transcriptional data to identify thresholds of effects in a human lens epithelial cell-line exposed to ionizing radiation. Int J Radiat Biol. 95(2):156–169. doi:10.1080/09553002.2019.1539883.

Crump KS. 1984. A new method for determining allowable daily intakes. Fundam Appl Toxicol. 4(5):854–871. doi:10.1016/0272-0590(84)90107-6.

Cui J, Yang G, Pan Z, Zhao Y, Liang X, Li W, Cai L. 2017. Hormetic response to low-dose radiation: focus on the immune system and its clinical implications. Int J Mol Sci. 18(2):280. doi:10.3390/ijms18020280.

da Veiga Leprevost F, Haynes SE, Avtonomov DM, Chang H, Shanmugam AK, Mellacheruvu D, Kong AT, Nesvizhskii AI. 2020. Philosopher: a versatile toolkit for shotgun proteomics data analysis. Nat Methods. 17(9):869–870. doi:10.1038/s41592-020-0912-y.

Everson TM, Marsit CJ. 2018. Integrating -omics approaches into human population-based studies of prenatal and early-life exposures. Curr Environ Health Rep. 5(3):328–337. doi:10.1007/s40572-018-0204-1.

Fang F, Yu X, Wang X, Zhu X, Liu L, Rong L, Niu D, Li J. 2022. Transcriptomic profiling reveals gene expression in human peripheral blood after exposure to low-dose ionizing radiation. J Radiat Res. 63(1):8–18. doi:10.1093/jrr/rrab091.

Food and Agriculture Organization of the United Nations and the World Health Organization. 2009. Principles and methods for the risk assessment of chemicals in food. https://iris.who.int/bitstream/handle/10665/44065/WHO_EHC_240_1_eng_front.pdf?sequence=1.

Gamble SC, Dunn MJ, Wheeler CH, Joiner MC, Adu-Poku A, Arrand JE. 2000. Expression of proteins coincident with inducible radioprotection in human lung epithelial cells. Cancer Res. 60(8):2146–2151. https://pubmed.ncbi.nlm.nih.gov/10786677/.

Giannattasio M, Lazzaro F, Plevani P, Muzi-Falconi M. 2005. The DNA damage checkpoint response requires histone H2B ubiquitination by Rad6-Bre1 and H3 methylation by Dot1. *J Biol Chem. 280(11):9879–9886. doi:10.1074/jbc.M414453200.

Haber LT, Dourson ML, Allen BC, Hertzberg RC, Parker A, Vincent MJ, Maier A, Boobis AR. 2018. Benchmark dose (BMD) modeling: current practice, issues, and challenges. Crit Rev Toxicol. 48(5):387–415. doi:10.1080/10408444.2018.1430121.

Hardy A, Benford D, Halldorsson T, Jeger MJ, Knutsen KH, More S, Mortensen A, Naegeli H, Noteborn H, Ockleford C, et al. 2017. Update: use of the benchmark dose approach in risk assessment. EFSA J. 15(1):e04658. doi:10.2903/j.efsa.2017.4658.

Højsgaard S, Halekoh U. 2023. doBy: groupwise statistics, LSmeans, linear estimates, utilities (4.6.21) [computer software]. https://cran.r-project.org/web/packages/doBy/index.html.

Isermann A, Mann C, Rübe CE. 2020. Histone variant H2A.J Marks persistent DNA damage and triggers the secretory phenotype in radiation-induced senescence. Int J Mol Sci. 21(23):9130. doi:10.3390/ijms21239130.

Ji K, Wang Y, Du L, Xu C, Liu Y, He N, Wang J, Liu Q. 2019. Research progress on the biological effects of low-dose radiation in China. Dose Response. 17(1):1559325819833488. doi:10.1177/1559325819833488.

Joiner MC, Marples B, Lambin P, Short SC, Turesson I. 2001. Low-dose hypersensitivity: current status and possible mechanisms. Int J Radiat Oncol Biol Phys. 49(2):379–389. doi:10.1016/S0360-3016(00)01471-1.

Karami V, Gholami M. 2018. Addressing as low as reasonably achievable (ALARA) in pediatric computed tomography (CT) procedures. J Res Med Dent Sci. 6:104–114. https://www.semanticscholar.org/paper/Addressing-as-Low-as-Reasonably-Achievable-(ALARA)-Karami-Gholami/589528b03675d90888eda26bf388049d12adf59c.

Karimi G, Balali-Mood M, Alamdaran S, Badie-Bostan H, Mohammadi E, Ghorani-Azam A, Sadeghi M, Riahi-Zanjani B. 2017. Increase in the Th1-cell-based immune response in healthy workers exposed to low-dose radiation - immune system status of radiology staff. J Pharmacopuncture. 20(2):107–111. doi:10.3831/KPI.2017.20.014.

Kong AT, Leprevost FV, Avtonomov DM, Mellacheruvu D, Nesvizhskii AI. 2017. MSFragger: ultrafast and comprehensive peptide identification in shotgun proteomics. Nat Methods. 14(5):513–520. doi:10.1038/nmeth.4256.

Koryakina E, Potetnya VI, Troshina M, Baykuzina R, Koryakin S, Lychagin A, Solovev A, Saburov V, Pikalov V, Shegay P, et al. 2022. Hypersensitivity and induced radioresistance in Chinese hamster cells exposed to radiations with different LET values. Int J Mol Sci. 23(12):6765. doi:10.3390/ijms23126765.

Kuikka JT. 2009. Low-dose radiation risk and the linear no-threshold model. Int J Low Radiat. 6(2):157. doi:10.1504/IJLR.2009.028534.

Lacombe J, Sima C, Amundson SA, Zenhausern F. 2018. Candidate gene biodosimetry markers of exposure to external ionizing radiation in human blood: a systematic review. PLoS One. 13(6):e0198851. doi:10.1371/journal.pone.0198851.

Laurier D, Billarand Y, Klokov D, Leuraud K. 2023. The scientific basis for the use of the linear no-threshold (LNT) model at low doses and dose rates in radiological protection. J Radiol Prot. 43(2):024003. doi:10.1088/1361-6498/acdfd7.

Laurier D, Rühm W, Paquet F, Applegate K, Cool D, Clement C, International Commission on Radiological Protection (ICRP). 2021. Areas of research to support the system of radiological protection. Radiat Environ Biophys. 60(4):519–530. doi:10.1007/s00411-021-00947-1.

Lee K, Weng JT, Hsu PW, Chi Y, Chen C, Liu IY, Chen Y, Wu LS. 2014. Gene expression profiling of biological pathway alterations by radiation exposure. Biomed Res Int. 2014:834087. doi:10.1155/2014/834087.

Little MP, Muirhead CR. 1996. Evidence for curvilinearity in the cancer incidence dose-response in the Japanese atomic bomb survivors. Int J Radiat Biol. 70(1):83–94. doi:10.1080/095530096145364.

Liu Z, Cologne J, Amundson SA, Noda A. 2023. Candidate biomarkers and persistent transcriptional responses after low and high dose ionizing radiation at high dose rate. Int J Radiat Biol. 99(12):1853–1864. doi:10.1080/09553002.2023.2241897.

Marples B, Joiner MC. 1993. The response of Chinese hamster V79 cells to low radiation doses: evidence of enhanced sensitivity of the whole cell population. Radiat Res. 133(1):41–51. https://pubmed.ncbi.nlm.nih.gov/8434112/. doi:10.2307/3578255.

Mattsson S, Nilsson M. 2015. On the estimation of radiation-induced cancer risks from very low doses of radiation and how to communicate these risks. Radiat Prot Dosimetry. 165(1-4):17–21. doi:10.1093/rpd/ncv037.

Narendran N, Luzhna L, Kovalchuk O. 2019. Sex difference of radiation response in occupational and accidental exposure. Front Genet. 10:260. doi:10.3389/fgene.2019.00260.

Nosel I, Vaurijoux A, Barquinero J, Gruel G. 2013. Characterization of gene expression profiles at low and very low doses of ionizing radiation. DNA Repair. 12(7):508–517. doi:10.1016/j.dnarep.2013.04.021.

Pečinka L, Moráň L, Kovačovicová P, Meloni F, Havel J, Pivetta T, Vaňhara P. 2024. Intact cell mass spectrometry coupled with machine learning reveals minute changes induced by single gene silencing. Heliyon. 10(9):e29936. doi:10.1016/j.heliyon.2024.e29936.

Pennington CW, Siegel JA. 2019. The linear no-threshold model of low-dose radiogenic cancer: a failed fiction. Dose Response. 17(1):1559325818824200. doi:10.1177/1559325818824200.

Phillips JR, Svoboda DL, Tandon A, Patel S, Sedykh A, Mav D, Kuo B, Yauk CL, Yang L, omas RS, et al. 2019. BMDExpress 2: enhanced transcriptomic dose-response analysis workflow. Bioinformatics. 35(10):1780–1782. doi:10.1093/bioinformatics/bty878.

Preston DL, Ron E, Tokuoka S, Funamoto S, Nishi N, Soda M, Mabuchi K, Kodama K. 2007. Solid cancer incidence in atomic bomb survivors: 1958-1998. Radiat Res. 168(1):1–64. doi:10.1667/RR0763.1.

Qutob SS, Chauhan V, Kuo B, Williams A, Yauk CL, McNamee JP, Gollapudi B. 2018. The application of transcriptional benchmark dose modeling for deriving thresholds of effects associated with solar-simulated ultraviolet radiation exposure. Environ Mol Mutagen. 59(6):502–515. doi:10.1002/em.22196.

Reardon AJF, Farmahin R, Williams A, Meier MJ, Addicks GC, Yauk CL, Matteo G, Atlas E, Harrill J, Everett LJ, et al. 2023. From vision toward best practices: evaluating in vitro transcriptomic points of departure for application in risk assessment using a uniform workflow. Front Toxicol. 5:1194895. doi:10.3389/ftox.2023.1194895.

Reed RP. 2024. Replace the linear no-threshold model with a risk-informed targeted approach to radiation protection. Health Phys. 126(6):374–385. doi:10.1097/HP.0000000000001803.

Repetto O, Caggiari L, De Zorzi M, Elia C, Mussolin L, Buffardi S, Pillon M, Muggeo P, Casini T, Steffan A, et al. 2022. Quantitative plasma proteomics to identify candidate biomarkers of relapse in pediatric/adolescent Hodgkin lymphoma. Int J Mol Sci. 23(17):9911. doi:10.3390/ijms23179911.

Roberts JA, Basu-Roy S, Shin J, Varma VR, Williamson A, Blackshear C, Griswold ME, Candia J, Elango P, Karikkineth AC, et al. 2024. Serum proteomic signatures of common health outcomes among older adults. Gerontology. 70(3):269–278. doi:10.1159/000534753.

Schmitz-Feuerhake I, Busby C, Pflugbeil S. 2016. Genetic radiation risks: a neglected topic in the low dose debate. Environ Health Toxicol. 31:e2016001. doi:10.5620/eht.e2016001.

Shaltiel IA, Krenning L, Bruinsma W, Medema RH. 2015. The same, only different – DNA damage checkpoints and their reversal throughout the cell cycle. J Cell Sci. 128(4):607–620. doi:10.1242/jcs.163766.

Shore RE, Beck HL, Boice JD, Caffrey EA, Davis S, Grogan HA, Mettler FA, Preston RJ, Till JE, Wakeford R, et al. 2019. Recent epidemiologic studies and the linear no-threshold model for radiation protection—considerations regarding NCRP commentary 27. Health Phys. 116(2):235–246. doi:10.1097/HP.0000000000001015.

Stainforth R, Vuong N, Adam N, Kuo B, Wilkins RC, Yauk C, Beheshti A, Chauhan V. 2022. Benchmark dose modeling of transcriptional data: a systematic approach to identify best practices for study designs used in radiation research. Int J Radiat Biol. 98(12):1832–1844. doi:10.1080/09553002.2022.2110300.

Tharmalingam S, Sreetharan S, Kulesza AV, Boreham DR, Tai TC. 2017. Low-dose ionizing radiation exposure, oxidative stress and epigenetic programing of health and disease. Radiat Res. 188(4.2):525–538. doi:10.1667/RR14587.1.

UNSCEAR. 2012. Sources, effects and risks of ionizing radiation. New York (NY): United Nations Publication; [retrieved 2025 Jan 22]. https://www.unscear.org/unscear/uploads/documents/unscear-reports/UNSCEAR_2012_Report-CORR.pdf.

UNSCEAR. 2021. Report of the United Nations Scientific Committee on the effects of atomic radiation. New York (NY): United Nations Publication; [retrieved 2025 Jan 14]. https://www.unscear.org/docs/GAreports/2021/2021_GA_A-76-46_E.pdf.

Verheijen MC, Meier MJ, Asensio JO, Gant TW, Tong W, Yauk CL, Caiment F. 2022. R-ODAF: Omics data analysis framework for regulatory application. Regul Toxicol Pharmacol. 131:105143. doi:10.1016/j.yrtph.2022.105143.

Vuong N, Khilji S, Williams A, Adam N, Flores D, Fulton KM, Baay I, Twine SM, Meier MJ, Kumarathasan P, et al. 2025. Integration of multi-omics and benchmark dose modeling to support adverse outcome pathways. Int J Radiat Biol. 101(3):240–253. doi:10.1080/09553002.2024.2442694.

Wakeford R. 2009. Radiation in the workplace-a review of studies of the risks of occupational exposure to ionising radiation. J Radiol Prot. 29(2A):A61–A79. doi:10.1088/0952-4746/29/2A/S05.

Wignall JA, Shapiro AJ, Wright FA, Woodruff TJ, Chiu WA, Guyton KZ, Rusyn I. 2014. Standardizing benchmark dose calculations to improve science-based decisions in human health assessments. Environ Health Perspect. 122(5):499–505. doi:10.1289/ehp.1307539.

Xie S, Wu H, Wang Q, Cogswell JP, Husain I, Conn C, Stambrook P, Jhanwar-Uniyal M, Dai W. 2001. Plk3 functionally links DNA damage to cell cycle arrest and apoptosis at least in part via the p53 pathway. *J Biol Chem. 276(46):43305–43312. doi:10.1074/jbc.M106050200.

Yu F, Haynes SE, Teo GC, Avtonomov DM, Polasky DA, Nesvizhskii AI. 2020. Fast quantitative analysis of timsTOF PASEF data with MSFragger and IonQuant. Mol Cell Proteomics. 19(9):1575–1585. doi:10.1074/mcp.TIR120.002048.

Yu F, Yu S, Duan L, Yang S, Hou X, Du Y, Gao M, Zuo J, Sun L, Fu X, et al. 2024. Proteomics sequencing reveals the role of TGF-β signaling pathway in the peripheral blood of offspring rats exposed to fluoride. Biol Trace Elem Res. 202(5):2100–2110. doi:10.1007/s12011-023-03805-x.

Zyla J, Finnon P, Bulman R, Bouffler S, Badie C, Polanska J. 2014. Seeking genetic signature of radiosensitivity–a novel method for data analysis in case of small sample sizes. Theor Biol Med Model. 11(Suppl 1):S2. doi:10.1186/1742-4682-11-S1-S2.